Inorg. Chem. **2008**, *47*, 4963−4976

Detailed Assignment of the Magnetic Circular Dichroism and UV−vis Spectra of Five-Coordinate High-Spin Ferric [Fe(TPP)(Cl)]

Florian Paulat and Nicolai Lehnert*

Department of Chemistry, The University of Michigan, 930 N. University Avenue, Ann Arbor, Michigan 48109-1055

Received February 13, 2008

High-spin (hs) ferric heme centers occur in the catalytic or redox cycles of many metalloproteins and exhibit very complicated magnetic circular dichroism (MCD) and UV−vis absorption spectra. Therefore, detailed assignments of the MCD spectra of these species are missing. In this study, the electronic spectra (MCD and UV−vis) of the five-coordinate hs ferric model complex [Fe(TPP)(Cl)] are analyzed and assigned for the first time. A correlated fit of the absorption and low-temperature MCD spectra of [Fe(TPP)(Cl)] lead to the identification of at least 20 different electronic transitions. The assignments of these spectra are based on the following: (a) variable temperature and variable field saturation data, (b) time-dependent density functional theory calculations, (c) MCD pseudo **A**-terms, and (d) correlation to resonance Raman (rRaman) data to validate the assignments. From these results, a number of puzzling questions about the electronic spectra of [Fe(TPP)(Cl)] are answered. The Soret band in [Fe(TPP)(Cl)] is split into three components because one of its components is mixed with the porphyrin $A_{2u}\langle 72\rangle \rightarrow E_g\langle 82/83\rangle$ ($\pi \rightarrow \pi^*$) transition. The broad, intense absorption feature at higher energy from the Soret band is due to one of the Soret components and a mixed σ and π chloro to iron CT transition. The high-temperature MCD data allow for the identification of the Q_v band at 20 202 cm^{-1}, which corresponds to the **C**-term feature at 20 150 cm^{-1}. Q is not observed but can be localized by correlation to rRaman data published before. Finally, the low energy absorption band around 650 nm is assigned to two P → Fe charge transfer transitions, one being the long sought after A_{1u}(HOMO) → d_π transition.

Introduction

Magnetic Circular Dichroism (MCD) spectroscopy is an extremely powerful technique to investigate the electronic structures and spectra of paramagnetic transition metal complexes.[1,2] This technique has clear advantages compared to UV−vis absorption spectroscopy because of the much better resolution of electronic transitions. Compared to Electron Paramagnetic Resonance (EPR), MCD is not restricted to noninteger spin systems. In addition, the polarizations of the electronic transitions are accessible by MCD in samples of randomly oriented molecules. Correspondingly, MCD spectroscopy has frequently been applied to heme proteins.[1c,f,3] Heme active sites occur in many different proteins and are extremely important for numerous biological processes.[4] Detailed information about the spin state, geometry, oxidation state (ferrous, ferric, and ferryl), and axial ligand (identity, number, and type) of the heme(s) in many different proteins has been obtained by comparison of their MCD data with those of standards, including

* To whom correspondence should be addressed. E-mail: lehnertn@umich.edu.

(1) (a) Stephens, P. J. *Annu. Rev. Phys. Chem.* **1974**, *25*, 201–232. (b) Stephens, P. J. *Adv. Chem. Phys.* **1976**, *35*, 197–264. (c) Cheesman, M. R.; Greenwood, C.; Thomson, A. J. *Adv. Inorg. Chem.* **1991**, *36*, 201–255. (d) Solomon, E. I.; Pavel, E. G.; Loeb, K. E.; Campochiaro, C. *Coord. Chem. Rev.* **1995**, *144*, 369–460. (e) Oganesyan, V. S.; George, S. J.; Cheesman, M. R.; Thomson, A. J. *J. Chem. Phys.* **1999**, *110*, 762–777. (f) Cheek, J.; Dawson, J. H. In *Handbook of Porphyrins and Related Macrocycles*; Kadish, K., Smith, K., Guilard, R., Eds.; Academic Press: New York, 2000; Vol. *7*, pp 339−369. (g) Lehnert, N.; DeBeer George, S.; Solomon, E. I. *Curr. Opin. Chem. Biol.* **2001**, *5*, 176–187.

(2) Neese, F.; Solomon, E. I. *Inorg. Chem.* **1999**, *38*,1847–1865.

(3) (a) Thomson, A. J.; Brittain, T.; Greenwood, C.; Springall, J. *FEBS Lett.* **1976**, *67*, 94–98. (b) Thomson, A. J.; Brittain, T.; Greenwood, C.; Springall, J. P. *Biochem. J.* **1977**, *165*, 327–336. (c) Thomson, A. J.; Johnson, M. K.; Greenwood, C.; Gooding, P. E. *Biochem. J.* **1981**, *193*, 687–697. (d) Roach, M. P.; Pond, A. E.; Thomas, M. R.; Boxer, S. G.; Dawson, J. H. *J. Am. Chem. Soc.* **1999**, *121*, 12088–12093. (e) Maranon, M. J. R.; Mercier, D.; van Huystee, R. B.; Stillman, M. J. *Biochem. J.* **1994**, *301*, 335.

(4) *Advances in Inorganic Biochemistry*; Eichhorn, G. L., Marzilli, L. G., Eds.; Elsevier: New York, 1988; Vol. *7*, Heme Proteins.

10.1021/ic8002838 CCC: $40.75
Published on Web 04/25/2008

porphyrin model complexes and heme proteins with known spectra. Hence, MCD has been widely used as a powerful "fingerprinting" technique to classify newly discovered heme proteins.[5,1f] For example, Dawson and Sono have used MCD spectroscopy to provide evidence for axial cysteine ligation to heme in the high-spin (hs) ferric state of cytochrome P450 and chloroperoxidase by comparing the MCD spectra of these enzymes to those of synthetic model compounds.[5]

In addition, the MCD spectra of newly discovered heme proteins are often compared to those of horseradish peroxidase (HRP) and myoglobin (Mb) to determine the nature of the prosthetic group and its ligation state, because these proteins have been extensively studied by MCD spectroscopy.[1f] Importantly, however, in almost all of these cases, detailed assignments of the MCD spectra are missing, and the nature of the different transitions observed is thus unknown. In particular, hs ferric hemes exhibit very complicated MCD and UV−vis absorption spectra.[1c,5] These species occur in the catalytic or redox cycles of many proteins and therefore play a significant role in enzymology. Important axial ligands to hs ferric hemes are cysteinate in P450 type enzymes, histidine in HRP, hemoglobin (Hb), Mb, and in nitrophorins from *Rhodnius prolixus*.[6] In addition, catalase enzymes contain a five-coordinate hs ferric heme b with tyrosinate ligation, which is also evident from MCD spectroscopy.[7] It is therefore of critical importance to explore the electronic structures of hs ferric heme active sites to understand their functions in these different proteins. One important step toward this goal is the actual assignment of their UV−vis and MCD spectra. The identification of axial ligand to iron charge transfer (CT) transitions in these systems will provide key insight into the heme−axial ligand interaction and how this allows for a fine-tuning of the properties of the heme. Besides the investigation of metalloporphyrins in biological systems, synthetic porphyrin model complexes have widely been studied to gain insight into the catalytic reactions or functions performed by heme proteins.[8] In many cases, tetraphenylporphyrin (TPP^{2-}) and octaethylporphyrin (OEP^{2-}) ligands have been used for such model systems.

To establish detailed assignments for the electronic spectra of a hs ferric heme for the first time, we have studied the five-coordinate model complex [Fe(TPP)(Cl)], which exhibits very complex MCD and UV−vis absorption spectra related to those of the hs ferric heme centers in the above-mentioned enzymes. Therefore, this complex is an excellent model for the five-coordinate hs ferric state in heme proteins. So far, no assignments of the MCD spectra of [Fe(TPP)(Cl)] have been made. Browett et al., who determined the zero-field splitting (zfs) parameter *D* for [Fe(TPP)(Cl)] by analyzing MCD saturation curves, stated in 1983,[9] "The analysis of the MCD [data] of FeCl(TPP) is therefore a substantial challenge. [•••] It remains to be demonstrated that this analysis successfully predicts the temperature dependence of the MCD to liquid helium temperatures, which is a sine qua non of a viable theory." This explicit theoretical description of MCD **C**-term intensity is now available via a general method developed by Neese and Solomon,[2,10] which we have applied in this study. Up to this day, the only effort to assign parts of the MCD spectra of [Fe(TPP)(Cl)] was performed by Kobayashi and co-workers.[11] Simple calculations were performed to investigate the effect of configuration interaction (CI) mixing of the porphyrin HOMOs (a_{1u} and a_{2u}) to d_π ($d_{xz,yz}$) CT states with the $\pi \rightarrow \pi^*$ Soret/Q excited states (singlet and triplet) of the porphyrin. However, as we will show in this work, this interpretation cannot account for the experimentally observed polarizations of many electronic transitions.

In summary, despite the large significance of hs ferric heme in biology, detailed assignments of MCD and UV−vis data of corresponding species are not available to this date. To this end, we have performed low-temperature MCD measurements on the five-coordinate model complex [Fe(TPP)(Cl)], which has very complex electronic spectra and hence is a very good system to develop an MCD methodology to analyze the spectra of hs ferric heme complexes in models and proteins. Variable temperature and variable field (VTVH) measurements have been used to determine the polarizations of most of the electronic transitions observed in the MCD spectra of this compound. In correlation to resonance Raman (rRaman) results and time-dependent density functional theory (TD-DFT) calculations, this allows for a detailed assignment of the optical spectra of [Fe(TPP)(Cl)] for the first time, and this way provides detailed insight into the electronic structure of hs five-coordinate ferric hemes. In future studies, the methodology developed here will be applied to ferric cytochrome P450 and corresponding model complexes [Fe(TPP)(SR)], where assignments of the electronic spectra are lacking.

Experimental and Computational Procedures

Syntheses. The complex [Fe(TPP)(Cl)] was synthesized using published procedures[12] and isolated as a microcrystalline solid. The identity of the compound was established using ^{1}H NMR, UV−vis absorption, IR, and MCD spectroscopy.

^{1}H NMR(400 MHz, $CDCl_3$): 81.6 (s, pyrrole-H), 13.6 and 12.4 (s, meso-H), 6.45 (s, para-H) and ~5.3 (broad, ortho-H).

Theoretical Background. The theoretical background of MCD spectroscopy was developed by Stephens in the 1970s and has been

(5) Dawson, J. H.; Sono, M. *Chem. Rev.* **1987**, *87*, 1255–1276.
(6) (a) Cheng, L.;Richter-Addo, G. B. In *The Porphyrin Handbook*; Kadish, K. H.,Smith, K. M.,Guilard, R., Eds.; Academic Press: San Diego, 2000; Vol. 4, pp 219−292. (b) Poulos, T. L. In *The Porphyrin Handbook*; Kadish, K. H.,Smith, K. M.,Guilard, R., Eds.; Academic Press: San Diego, 2000; Vol. 4, pp 189−218.
(7) Andersson, L. A.; Johnson, A. K.; Simms, M. D.; Willingham, T. R. *FEBS Lett.* **1995**, *370*, 97–100.
(8) Walker, F. A. In *Encyclopedia of Inorganic Chemistry*; King, R. B., Ed.; John Wiley & Sons: New York, 1994; Vol. *4*, pp 1785−1846.
(9) Browett, W. R.; Fucaloro, A. F.; Morgan, T. V.; Stephens, P. J. *J. Am. Chem. Soc.* **1983**, *105*, 1868–1872.
(10) Neese, F.; Solomon, E. I. *J. Am. Chem. Soc.* **1998**, *120*, 12829–12848.
(11) (a) Kobayashi, H. *Adv. Biophys.* **1975**, *8*, 191–222. (b) Kobayashi, H.; Higuchi, T.; Eguchi, K. *Bull. Chem. Soc. Jpn.* **1976**, *49*, 457–463. (c) Kobayashi, H.; Yanagawa, Y.; Osada, H.; Minami, S.; Shimizu, M. *Bull. Chem. Soc. Jpn.* **1973**, *46*, 1471–1479.
(12) Adler, A. D.; Longo, F. R.; Kampas, F.; Kim, J. *J. Inorg. Nucl. Chem.* **1970**, *32*, 2443–2445.

summarized in a number of reviews and articles.[1a,b,d,e,g,2,13,14] MCD spectroscopy measures the difference in intensity of left (lcp) and right (rcp) circularly polarized light in an applied, longitudinal field. MCD intensity is proportional to three different contributions, designated as MCD **A**-, **B**-, and **C**-terms (cf. eq 1).

$$I \sim \left[A_1\left(\frac{-\partial f(E)}{\partial E}\right) + \left(B_0 + \frac{C_0}{kT}\right) f(E)\right] \cdot B \qquad (1)$$

Here, I is the MCD intensity, T is the temperature, B is the magnetic field, and the function $f(E)$ represents the band shape of an absorption band. Importantly, the **A**- and **B**-terms are temperature independent, whereas the MCD **C**-term intensity is temperature dependent. Therefore, the most important mechanism at low temperature is the **C**-term. From eq 1, the MCD intensity increases linearly with the strength of the magnetic field (B). This strictly applies to the **A**- and **B**-terms. The **C**-term intensity arises from a degenerate ground state, which is split in the magnetic field because of the Zeeman effect as shown in Supporting Information Scheme S1. In general, degenerate ground states are due to spin degeneracy, and hence, only paramagnetic compounds exhibit **C**-term signals. At low temperatures, kT is in the order of the Zeeman splitting in the presence of a strong magnetic field, which leads to a larger population of the lower energy compared to the higher energy Zeeman sublevels of the ground-state corresponding to the Boltzmann distribution. Hence, the intensities of the rcp and lcp transitions do not cancel anymore, leading to an absorption band shape for the **C**-term. A further decrease of the temperature or an increase of the magnetic field results in an increase in the population of the lowest-energy sublevel, and therefore, the **C**-term MCD intensity also increases. If the higher energy sublevels are completely depopulated, the **C**-term intensity reaches its maximum value and it saturates. Importantly, the temperature and magnetic field dependent **C**-term intensity contains the complete information of the ground-state properties including g values and zfs parameters as well as the polarizations of the electronic transitions. All this information can be extracted by fitting these **C**-term saturation magnetization curves.

UV−vis Spectroscopy. Absorption spectra were recorded in chloroform at room temperature using an Analytik Jena Specord S600 spectrophotometer. The absorption data were scaled using literature extinction coefficients (λ_{max} (ε in cm^{-1} M^{-1}) = 372 nm (4.71×10^4), 418 (1.08×10^5), 507 (1.18×10^4), 572 (5.0×10^3), and 685 (3.1×10^3)).[9]

MCD Spectroscopy. MCD spectra have been obtained on thin polystyrene (PS) films. The films were prepared by dissolving [Fe(TPP)(Cl)] and PS in benzene, followed by slow evaporation of the solvent. The PS films were placed between two quartz plates (Suprasil 1), which were mounted on a copper sample holder. MCD spectra were recorded using a setup that consists of an OXFORD SM^{4000} cryostat and a JASCO J810 CD spectropolarimeter. The SM^{4000} consists of a split pair superconducting magnet providing horizontal magnetic fields of 0−7 T in a low boil-off helium cryostat. The light source of the J810 is an air cooled xenon lamp. The detector system corresponds to two interchangeable head-on photomultiplier tubes. Samples are loaded into a 1.5−300 K variable temperature insert (VTI), which offers access to the sample by four optical windows made from Spectrosil B quartz. The obtained MCD spectra were measured in [θ] = mdeg and converted to $\Delta\varepsilon$ [M^{-1} T^{-1} cm^{-1}] using the conversion factor $\Delta\varepsilon = \theta/(32980 \cdot c \cdot d \cdot B)$, where c is the concentration, B is the magnetic field, and d is the thickness of the sample (path length). Importantly, the product $c \cdot d$ can be substituted by $A_{MCD}/\varepsilon_{UV-vis}$, where A is the absorbance of the sample measured by the CD spectrometer. This is of particular importance because it is difficult to determine d for the PS films used here. The extinction coefficient ε_{UV-vis} has been determined by Browett et al.[9] We have used ε_{UV-vis} and A determined for the Soret band for the calculation of the molar MCD intensity. For each temperature and field, the complete spectrum was recorded to obtain the VTVH data for all MCD bands and also to examine the quality of the spectra (baseline shifts, etc.). The smallest number of bands has been used for the deconvolution analysis of the MCD and UV−vis spectra of [Fe(TPP)(Cl)], and the quality of the individual fits has been checked using χ^2. Bandwiths and band centers were allowed to vary by 5% between MCD and UV-vis because of the different experimental conditions applied.

Density Functional Calculations. DFT calculations using Becke's three parameter hybrid functional with the correlation functional of Lee, Yang, and Parr (B3LYP)[15] were performed using the program package Gaussian 03.[16] The structure of [Fe(TPP)(Cl)] (S = 5/2) was fully optimized without simplifications using the LanL2DZ* basis set. The LanL2DZ* basis set consists of LanL2DZ plus polarization functions (from TZVP) on all heavy atoms.[17] TD-DFT calculations for [Fe(TPP)(Cl)], [Zn(P)], and [Zn(TPP)] applying B3LYP/LanL2DZ* were performed using G03. Calculations for [Fe(TPP)(Cl)] were performed both on the fully optimized structure and on a corresponding structure where the Fe−Cl distance has been set to the crystallographically obtained value of 2.192 Å determined by Hoard et al.[18] In all calculations, convergence was reached when the relative change in the density matrix between subsequent iterations was less than 1×10^{-8}. The absorption spectra of [Zn(P)] and [Zn(TPP)] were also calculated using the semiempirical INDO/S−CI method as implemented in ORCA.[19] In the case of [Fe(TPP)(Cl)], however, this method could not be applied because the wrong ground-state is predicted by INDO/S for this compound. Note that the number of states for the TD-DFT calculations on [Fe(TPP)(Cl)] was limited to 70 because of the complexity of the problem, which makes these calculations very time-consuming (keeping in mind the size of the molecule). Hence, the calculations cover the range up to 27 964 cm^{-1} (358 nm), and accordingly, higher energy states are not included in the analysis.

Fitting of the MCD VTVH Data. The VTVH data were fitted using the general method developed by Neese and Solomon.[2] The analysis is based on the following equation (2):

$$\frac{\Delta\varepsilon}{E} = \frac{\gamma}{4\pi S}\int_0^{\pi}\int_0^{2\pi}\sum_i N_i\left(l_x\langle S_x\rangle_i M_{yz}^{eff} + l_y\langle S_y\rangle_i M_{xz}^{eff} + l_z\langle S_z\rangle_i M_{xy}^{eff}\right)\sin(\theta)\,d\theta\,d\varphi \qquad (2)$$

where $\Delta\varepsilon/E$ is the MCD intensity, M^{eff} are the effective transition dipole moment products, $l_{x,y,z}$ describe the orientation of the magnetic field relative to the molecular coordinate system, N_i are the Boltzmann populations, and S_i are the spin-expectation values. The individual polarizations of the MCD bands can then be

(13) (a) Stephens, P. J. *J. Chem. Phys.* **1970**, *52*, 3489–3516. (b) Piepho, S. B.; Schatz, P. N. *Group Theory in Spectroscopy with Applications to Magnetic Circular Dichroism*; John Wiley & Sons: New York, 1983.

(14) Mack, J.; Stillman, M. J.; Kobayashi, N. *Coord. Chem. Rev.* **2007**, *25*, 1429–453.

(15) (a) Becke, A. D. *Phys. Rev. A* **1988**, *38*, 3098. (b) Becke, A. D. *J. Chem. Phys.* **1993**, *98*, 1372. (c) Becke, A. D. *J. Chem. Phys.* **1993**, *98*, 5648.

(16) Frisch M. J. et al. *Gaussian 03*; Gaussian, Inc.: Pittsburgh, PA, 2003.

(17) Praneeth, V. K. K.; Näther, C.; Peters, G.; Lehnert, N. *Inorg. Chem.* **2006**, *45*, 2795–2811.

(18) Hoard, J. L.; Cohen, G. H.; Glick, M. D. *J. Am. Chem. Soc.* **1967**, *89*, 1992–1996.

(19) Neese, F. *ORCA*, version 2.4; Universität Bonn: Bonn, Germany, 2004.

calculated using the M^{eff} values obtained from the fit of the VTVH saturation curves, using the equation (3):

$$\%x = 100\frac{(M_{xy}^{eff}\cdot M_{xz}^{eff})^2}{(M_{xy}^{eff}\cdot M_{xz}^{eff})^2+(M_{xy}^{eff}\cdot M_{yz}^{eff})^2+(M_{xz}^{eff}\cdot M_{yz}^{eff})^2} \quad (3)$$

The calculation of the *y*- and *z*-polarizations is performed correspondingly.

Results and Analysis

A. TD-DFT Calculations and Classification of the Electronic Transitions. A.1 Method Calibration for Quantum-Chemical Excited State Calculations Using Four-Coordinate Zinc Porphyrins: [Zn(P)] and [Zn(TPP)]. To explore the performance of TD-DFT and semiempirical INDO/S−CI calculations on metalloporphyrins, we have calculated the absorption spectra of the simple [Zn(P)] (P^{2-} = porphine) and [Zn(TPP)] (TPP^{2-} = tetraphenylporphyrin) complexes first and compared the results to the experimental spectra of [Zn(TPP)],[20] which shows very simple absorption spectra. These calculations lead to two important conclusions: (a) the simple porphine ligand is not a good model for TPP in both the TD-DFT and INDO/S−CI calculations, producing significant errors in comparison with experiment, and (b) more accurate results are obtained by adding polarization functions (from TZVP) to the LanL2DZ basis set on all heavy atoms (LanL2DZ* basis set).[17] A further extension of the basis set to TZVP does not lead to a noticeable improvement (cf. Supporting Information Table S1). These results are described in the Supporting Information.

A.2 Classification of the Electronic Transitions of [Fe(TPP)(Cl)]. A good theoretical description of the $[Fe(TPP)]^+$ core of [Fe(TPP)(Cl)] has been obtained using B3LYP with both LanL2DZ (cf. ref 21) and LanL2DZ* (this work) basis sets. However, both methods show large deviations from experiment with respect to the Fe−Cl bond length. From X-ray crystallography, d(Fe−Cl) = 2.192 Å[18] has been determined. In comparison, using B3LYP/LanL2DZ, d(Fe−Cl) = 2.32 Å is calculated. A better description of the Fe−Cl bond is obtained by adding polarization functions on all heavy atoms, which leads to d(Fe−Cl) = 2.26 Å. Therefore, we used the B3LYP/LanL2DZ* fully optimized structure for the TD-DFT calculations, but adjusted the Fe−Cl distance to the experimental value. For the evaluation of the TD-DFT results, it is first necessary to consider the molecular orbital (MO) diagram of [Fe(TPP)(Cl)]. Because this complex is hs (S = 5/2), all α-d orbitals are fully occupied, whereas the β-d orbitals are empty, leading to a $^6A_1$ ground state. Correspondingly, no CT transitions of porphyrin → Fe-d type are possible for α-electrons, and hence, only the β-orbitals are considered in the following analysis. Figure 1 shows the molecular orbital scheme for [Fe(TPP)(Cl)]. The corresponding charge contributions of the β-spin molecular orbitals are given in Table 1. Contour plots of important orbitals are shown in Figure 2. Note that the labels of the porphyrin π and π^* orbitals refer to the MO diagram of free porphine^{2-}, which is shown in Supporting Information Figure S1. In the applied coordinate system, the *z* axis is aligned with the Fe−Cl bond, whereas the *x* and *y* axes are located along the Fe−N bonds of the porphyrin ligand (cf. Figure 1, top). Correspondingly, the $d_{x^2-y^2}$ orbital of the metal forms a strong σ-bond with the pyrrole nitrogens of the porphyrin, whereas the d_{xy} orbital is practically nonbonding (lowest unoccupied molecular orbital, LUMO: $\beta\langle 170\rangle$). The $E_g\langle 82/83\rangle$ LUMOs of the free porphyrin ligand are mixed with d_{xz} and d_{yz} (labeled d_π) in [Fe(TPP)(Cl)] and have about 18% d_π contribution ($\beta\langle 174/175\rangle$; cf. Table 1). The metal-chloride σ-bond is mediated by the d_{z^2} orbital of iron and the p_z orbital of the chloro ligand. The corresponding bonding combination, p_z _ d_{z^2} ($\beta\langle 148\rangle$), has 24% iron d_{z^2} and 60% chloro p_z character, which corresponds to a strong σ bond.[21] Additional π-bonds between the d_{xz} and d_{yz} orbitals of iron and the p_x and $p_y$orbitals of the chloro ligand, respectively, are also present. The corresponding bonding combinations, p_y _ d_{yz} and p_x _ d_{xz} ($\beta\langle 152/153\rangle$), have about 8% metal and 46% chloride character (cf. Table 1), indicative of a medium strong interaction. The HOMOs of [Fe(TPP)(Cl)] are the $A_{1u}\langle 79\rangle$ and $A_{2u}\langle 81\rangle$ orbitals of the porphyrin core. Note that the A_{1u} orbital is mixed with the empty d_{z^2} _ p_z orbital (the antibonding combination of d_{z^2} and p_z of chloride). Other important molecular orbitals for the interpretation of the electronic spectra of [Fe(TPP)(Cl)] are low lying (occupied) porphyrin π orbitals, that is, $B_{2u}\langle 74\rangle$ ($\beta\langle 167\rangle$) and $A_{2u}\langle 72\rangle$ ($\beta\langle 156\rangle$). Note that the principal bonding scheme of [Fe(TPP)(Cl)], focusing on the metal-porphyrin interaction, has been analyzed before by Cheng et al.[22] A more detailed description of the Fe−Cl bond has recently been published by our group.[21] By using polarized rRaman spectroscopy, we have shown in this publication that the $[Fe(TPP)]^+$ core of [Fe(TPP)(Cl)] still behaves as if it has D_{4h} symmetry. Therefore, an effective D_{4h} symmetry is applied in the following analysis of the TD-DFT results.

The absorption and MCD spectra of [Fe(TPP)(Cl)] presented in Figure 3 are significantly more complex than those of [Zn(TPP)].[23] This is due to the hs d^5 configuration of iron(III), which leads to a $[d_{xz}, d_{yz}, d_{xy}, d_{z^2}, d_{x^2-y^2}]^5$ electron configuration as described above. Hence, all five d orbitals are singly occupied, which allows for a magnitude of CT transitions of porphyrin → Fe(III) and Cl^- → Fe(III) type. These are not present in Zn(II) with a d^{10} electron configuration. Scheme 1 shows all important electric dipole allowed transitions identified from TD-DFT. In the following, transitions are classified as inner porphyrin, porphyrin to iron CT (P → Fe CT), and chloro to iron CT transitions (Cl → Fe CT) for their further evaluation. Considering d−d transitions, these are all spin forbidden because of the $^6A_1$ ground-state of hs iron(III) and hence are not further considered. The following one-electron transitions are important:

(20) Edwards, L.; Dolphin, D. H.; Gouterman, M.; Adler, A. D. *J. Mol. Spectrosc.* **1971**, *38*, 16–32.

(21) Paulat, F.; Praneeth, V. K. K.; Näther, C.; Lehnert, N. *Inorg. Chem.* **2006**, *45*, 2835–2856.

(22) Cheng, R.-J.; Chen, P. Y.; Novell, T.; Liu, T.; Noddleman, L.; Case, D. A. *J. Am. Chem. Soc.* **2003**, *125*, 6774–6783.

(23) Gouterman, M. In *The Porphyrins*; Dolphin, D., Ed.; Academic Press: New York, 1979; Vol. *III*, Part A, pp. 1−156.

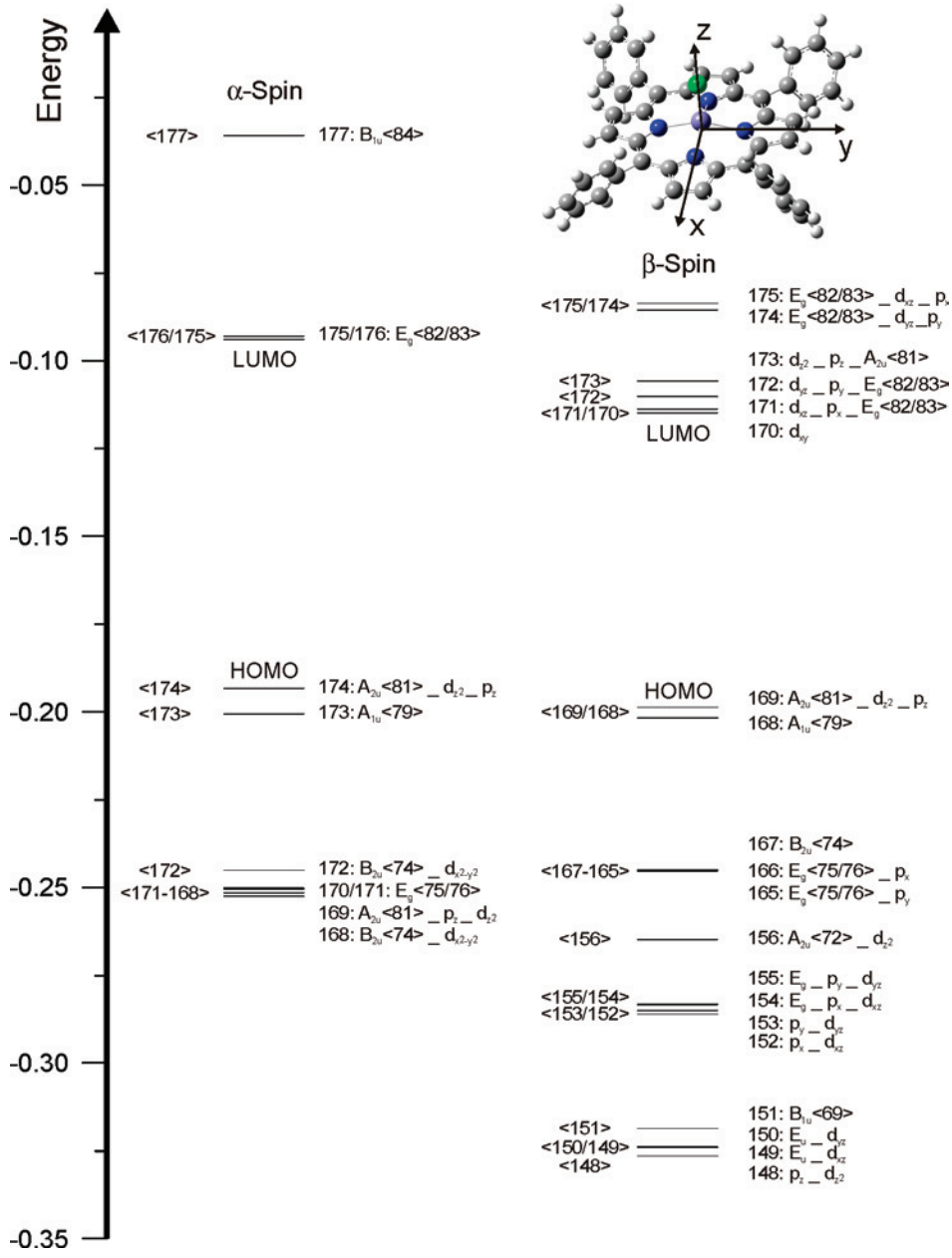

Figure 1. Molecular orbital diagram of [Fe(TPP)(Cl)] calculated with B3LYP/LanL2DZ* (*d*(Fe−Cl) is taken from the crystal structure; ref 18). Note that p_x, p_y, and p_z are chloride 3p orbitals. The labels of the porphyrin orbitals, for example $A_{2u}\langle 81\rangle$, refer to Supporting Information Figure S1. Molecular orbital labels *a* _ *b* indicate that orbital *a* interacts with *b* and that *a* has a larger contribution to the resulting MO.

(1) Inner porphyrin transitions (cf. Scheme 1 and Supporting Information Figure S1 for porphyrin orbital labels)
(a) $\pi \rightarrow \pi^{*\,(0)}$: A_{1u}, $A_{2u}\langle 79,81\rangle \rightarrow E_g\langle 82,83\rangle$ (Soret and Q-band)
(b) $\pi \rightarrow \pi^{*\,(1)}$: $A_{2u}\langle 72\rangle \rightarrow E_g\langle 82,83\rangle$
(c) $\pi \rightarrow \pi^{*\,(2)}$: $B_{2u}\langle 74\rangle \rightarrow E_g\langle 82,83\rangle$

(2) Porphyrin to iron charge-transfer transitions (P → Fe CT; cf. Scheme 1)
(a) $CT^{(1)}$: $A_{1u}\langle 79\rangle \rightarrow d_{xz},d_{yz} = d_\pi$
(b) $CT^{(2)}$: $A_{2u}\langle 81\rangle \rightarrow d_{xz},d_{yz} = d_\pi$
(c) $CT^{(3)}$: $B_{2u}\langle 74\rangle \rightarrow d_{xz},d_{yz} = d_\pi$
(d) $CT^{(4)}$: $A_{2u}\langle 72\rangle \rightarrow d_{xz},d_{yz} = d_\pi$
(e) $CT^{(5)}$: $A_{2u}\langle 81\rangle$ _ d_{z^2} _ $p_z \rightarrow d_{z^2}$ _ p_z _ $A_{2u}\langle 81\rangle$ (*z*-polarized)
(f) $CT^{(6)}$: $B_{2u}\langle 74\rangle \rightarrow d_{z^2}$ _ p_z _ $A_{2u}\langle 81\rangle$ (*z*-polarized)

Note that the overlap of the porphyrin orbital $A_{1u}\langle 79\rangle$ with the d_π orbitals of iron(III) is poor because the nitrogen p orbitals of the porphyrin do not contribute to $A_{1u}\langle 79\rangle$. Therefore, one would expect that $CT^{(1)}$ has no intensity. However, the d_π orbitals show mixing with the E_g ⟨82/83⟩ LUMO of the porphyrin dianion (∼18%, cf. Table 1), and therefore, $CT^{(1)}$ steals intensity from the intense $\pi \rightarrow \pi^*$ transition through this mixing.

3) Chloro to iron CT transitions (Cl → Fe CT; cf. Scheme 1)
(a) $CT^{(Cl,p)}$: p_x,$p_y \rightarrow d_\pi$ (*z*-polarized)
(b) $CT^{(Cl,\sigma)}$: $p_z \rightarrow d_{z^2}$ (*z*-polarized)

Importantly, all of the listed $\pi \rightarrow \pi^*$ inner porphyrin and P → Fe CT excited states with the exception of $CT^{(5,6)}$ have E_u symmetry, correspond to *x*,*y*-polarized transitions and are potentially subject to strong configuration interaction. In addition, note that the iron d_π orbitals and the $E_g\langle 82/83\rangle$ LUMO of the porphyrin are of the same symmetry and are

Table 1. Charge Contributions to the β Spin Molecular Orbitals of [Fe(TPP)(Cl)] Calculated with B3LYP/LanL2DZ* [a]

no.	label[b]	energy [Hartree]	Fe, d	Cl, p	porphyrin
$\beta\langle 177\rangle$	$B_{1u}\langle 84\rangle$	−0.03459	0	0	100
$\beta\langle 176\rangle$	$d_{x^2-y^2}$ _ $B_{1g}\langle 80\rangle$	−0.06626	53	0	47
$\beta\langle 175\rangle$	$E_g\langle 82/83\rangle$ _ d_{xz} _ p_x	−0.08372	17	1	82
$\beta\langle 174\rangle$	$E_g\langle 82/83\rangle$ _ d_{yz} _ p_y	−0.08563	18	1	81
$\beta\langle 173\rangle$	d_{z^2} _ p_z _ $A_{2u}\langle 81\rangle$	−0.10595	57	14	27
$\beta\langle 172\rangle$	d_{yz} _ p_y _ $E_g\langle 82/83\rangle$	−0.11024	57	6	35
$\beta\langle 171\rangle$	d_{xz} _ p_x _ $E_g\langle 82/83\rangle$	−0.11373	59	8	32
$\beta\langle 170\rangle$ LUMO	d_{xy}	−0.11496	93	0	6
$\beta\langle 169\rangle$ HOMO	$A_{2u}\langle 81\rangle$ _ d_{z^2} _ p_z	−0.19876	9	2	87
$\beta\langle 168\rangle$	$A_{1u}\langle 79\rangle$	−0.20181	0	0	100
$\beta\langle 167\rangle$	$B_{2u}\langle 74\rangle$	−0.24501	0	0	100
$\beta\langle 166\rangle$	$E_g\langle 75/76\rangle$ _ p_x	−0.24520	0	14	85
$\beta\langle 165\rangle$	$E_g\langle 75/76\rangle$ _ p_y	−0.24535	0	12	86
$\beta\langle 157-164\rangle$	Phenyl(π)	−0.25168 to −0.26025			
$\beta\langle 156\rangle$	$A_{2u}\langle 72\rangle$ _ d_{z^2}	−0.26481	4	0	94
$\beta\langle 155\rangle$	$E_g\langle 75/76\rangle$ _ p_y _ d_{yz}	−0.28322	2	10	84
$\beta\langle 154\rangle$	$E_g\langle 75/76\rangle$ _ p_x _ d_{xz}	−0.28349	3	14	82
$\beta\langle 153\rangle$	p_y _ d_{yz}	−0.28512	8	48	40
$\beta\langle 152\rangle$	p_x _ d_{xz}	−0.28606	8	43	46
$\beta\langle 151\rangle$	$B_{1u}\langle 69\rangle$	−0.31854	0	0	100
$\beta\langle 150\rangle$	E_u _ d_{yz}	−0.32385	3	0	97
$\beta\langle 149\rangle$	E_u _ d_{xz}	−0.32412	2	0	98
$\beta\langle 148\rangle$	p_z _d_{z^2}	−0.32644	24	60	12

[a] d(Fe−Cl) is taken from the crystal structure; ref 18. [b] p_x, p_y, and p_z are the chloride 3p orbitals. The labels of the porphyrin orbitals, for example $A_{2u}\langle 81\rangle$, refer to Supporting Information Figure S1.

therefore mixed (cf. Table 1). Correspondingly, the electronic transitions observed in [Fe(TPP)(Cl)] are also highly mixed as evident from the TD-DFT results, which renders the quantitative analysis of these spectra highly challenging. Supporting Information Table S2 lists all important excited states obtained from the TD-DFT calculations and their individual contributions. Scheme 1 summarizes the most important transitions.

A.3 Principal Trends in the Electronic Spectra of [Fe(TPP)(Cl)]. The TD-DFT calculations show out-of-plane (z-polarized) transitions at 11945, 12325, 20740, 22455, 22605 and 25008 cm^{-1} originating from the z-polarized excited states $CT^{(Cl,\pi,\sigma)}$ and $CT^{(5,6)}$ (cf. Supporting Information Table S2), respectively. Note that both $CT^{(5,6)}$ are z-polarized because of the out-of-plane displacement of the iron center toward the axial chloro ligand in [Fe(TPP)(Cl)]. Importantly, the z-polarized bands are all calculated to lower energy of the Soret band. Eaton and Hochstrasser observed a weak z-polarized band ($\varepsilon = 800\ M^{-1}\ cm^{-1}$) at 14388 cm^{-1} (695 nm) in the polarized single crystal UV−vis absorption spectrum of ferricytochrome c, which contains low-spin (ls) Fe(III) and has an $S = 1/2$ ground state. They assigned this band to $CT^{(5)}$.[24] In comparison, the TD-DFT calculations predict $CT^{(5)}$ in hs [Fe(TPP)(Cl)] at 11945 cm^{-1} (837 nm), which is an almost pure excited state (82% $CT^{(5)}$ character). The transition at 12325 cm^{-1} (811 nm) corresponds to $A_{1u}\langle 79\rangle \rightarrow d_{xy}$ (90% contribution) with about 10% $CT^{(5)}$ character. Correspondingly, this feature has almost no absorption intensity because of poor orbital overlap of $A_{1u}\langle 79\rangle$ and d_{xy}. The next z-polarized bands to higher energy are found at 20740 cm^{-1} and 22455 cm^{-1}. Both correspond to Laporte forbidden $E_g \rightarrow d_\pi$ transitions (about 90% contribution; cf. Supporting Information Table S2). Their weak intensity and z-polarization is due to admixture of 7% chloro to iron π CT ($CT^{(Cl,\pi)}$), 4% $CT^{(Cl,\sigma)}$, and 6% $CT^{(6)}$, respectively. The corresponding almost pure $CT^{(6)}$ transition (90%) is predicted very close in energy at 22605 cm^{-1}. Finally, the z-polarized transition calculated at highest energy is located at 25008 cm^{-1}. This feature corresponds to a mixed chloro to iron and porphyrin to iron CT transition with about 39% $CT^{(Cl,\pi)}$, 13% $CT^{(Cl,\sigma)}$, and 28% $CT^{(5)}$ contribution.

Importantly, all other excited states below 20000 cm^{-1} (500 nm) derive from mixing of $\pi \rightarrow \pi^{*(0)}$ (Q/Soret band) with either $CT^{(1)}$ or $CT^{(2)}$. Mixing of $\pi \rightarrow \pi^{*(0)}$ with $CT^{(2)}$ leads to very weak features at 8342, 8800, 18988, and 18990 cm^{-1}, as listed in Supporting Information Table S2. Interestingly, $CT^{(2)}$ is almost exclusively mixed with the $A_{2u} \rightarrow E_g$ component of $\pi \rightarrow \pi^{*(0)}$, whereas $CT^{(1)}$ mixes with both the A_{1u} and $A_{2u} \rightarrow E_g$ transitions of $\pi \rightarrow \pi^{*(0)}$. The latter interaction gives rise to bands at 12329, 12910, 13893, 14185, 16783, and 16921 cm^{-1} as listed in Supporting Information Table S2.

The region above 20000 cm^{-1} contains a number of new electronic transitions. $CT^{(3)}$ is observed at 21631 cm^{-1} (462 nm) and 22341 cm^{-1} (448 nm). Both states have about 89% $CT^{(3)}$ character and are mixed with $\pi \rightarrow \pi^{*(0)}$ (∼5%) and $\pi \rightarrow \pi^{*(2)}$ (2%). $CT^{(4)}$, which originates from the low lying $A_{2u}\langle 72\rangle$ porphyrin orbital, is predicted at 25202 cm^{-1} (397 nm). Further excited states with $CT^{(4)}$ contribution are calculated at 24410 cm^{-1} (410 nm) and 24446 cm^{-1} (409 nm). These two excited states have mainly $p_{x,y}(Cl) \rightarrow d_{z^2}$ character (53%; cf. Supporting Information Table S2), which, however, are overlap forbidden transitions that do not contribute to the oscillator strengths of these features. The calculated relatively large intensities of these transitions are actually due to substantial admixture of the allowed $\pi \rightarrow \pi^{*(0)}$ (21%) and $\pi \rightarrow \pi^{*(2)}$ (6%) transitions. Four excited states with significant $\pi \rightarrow \pi^{*(2)}$ character are located at

(24) Eaton, W. A.; Hochstrasser, R. M. *J. Chem. Phys.* **1967**, *46*, 2533–2539.

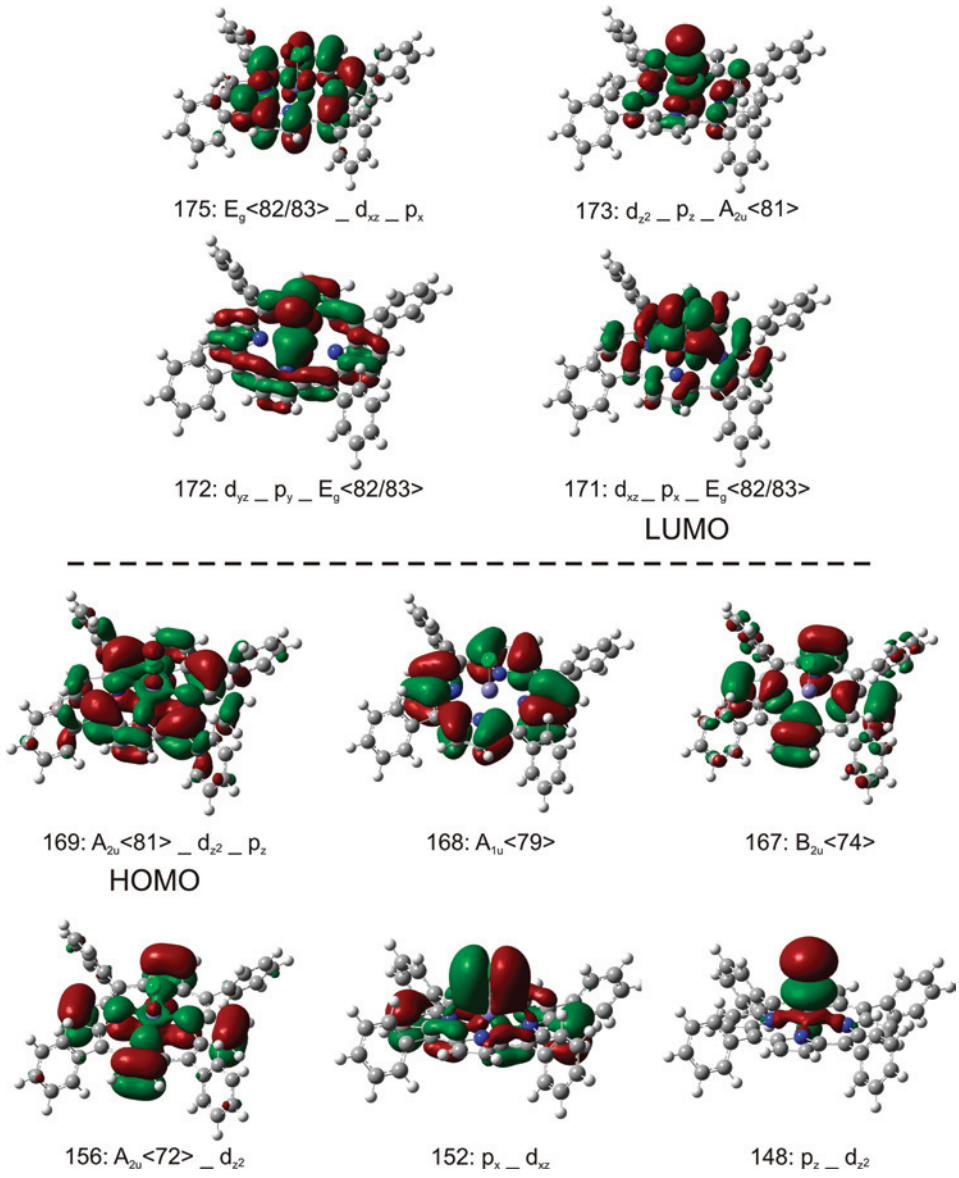

Figure 2. Contour plots of important molecular β orbitals of [Fe(TPP)(Cl)] (B3LYP/LanL2DZ*, d(Fe−Cl) is taken from the crystal structure; ref 18). For the labels see Figure 1.

25475, 25718, 27164, and 27250 cm^{-1} (cf. Supporting Information Table S2). The former two transitions show mixing with $CT^{(2,3)}$.

In the Soret region, four intense transitions are calculated within 300 cm^{-1} (transitions 24−27 in Supporting Information Table S2). State 24 at 25843 cm^{-1} corresponds to a $\pi \rightarrow \pi^{*(1)}$ transition (31%) with about 6% $\pi \rightarrow \pi^{*(0)}$ (Soret) contribution. Transitions 25 and 26 (at 26071 and 26109 cm^{-1}), corresponding to the Soret components 1 and 2 with 14 and 11% $\pi \rightarrow \pi^{*(0)}$ character, respectively, show significant admixtures of $\pi \rightarrow \pi^{*(2)}$ (about 20%) and $CT^{(4)}$ (11 and 34%, respectively). Finally, the third Soret component at 26143 cm^{-1} is again mixed with $\pi \rightarrow \pi^{*(2)}$ but does not show any $CT^{(4)}$ contribution (cf. Supporting Information Table S2).

Figure 5 shows a comparison of the observed and calculated absorption spectrum of [Fe(TPP)(Cl)]. As evident from this Figure, the TD-DFT calculations show surprisingly good agreement with experiment, but the alignment of the observed features is not close enough for a quantitative assignment of the electronic spectra. However, as elaborated above, the calculations help to classify the possible excited states, define their relative energies and intensities, and this way, provide very important input for the spectral assignments. In addition, the calculations afford a theoretical description of the z-polarized bands, which can experimentally be determined from fitting the VTVH data (vide infra). Hence, the TD-DFT results presented above serve as a basis for the interpretation of the experimental UV−vis and MCD data of [Fe(TPP)(Cl)].

B. Analysis of the MCD and UV−vis Spectra. B.1. Absolute A- and C-Term MCD Intensities. Figure 3 presents the UV−vis (top) and MCD **C**-term (bottom) spectra of [Fe(TPP)(Cl)] in molar units (ε, M^{-1} cm^{-1}, and $\Delta\varepsilon$, M^{-1} cm^{-1} T^{-1}, respectively). Both spectra are complicated, showing at least six bands in the UV−vis and 20 bands in the MCD spectrum, which again emphasizes the impact of MCD compared to absorption spectroscopy for the resolution

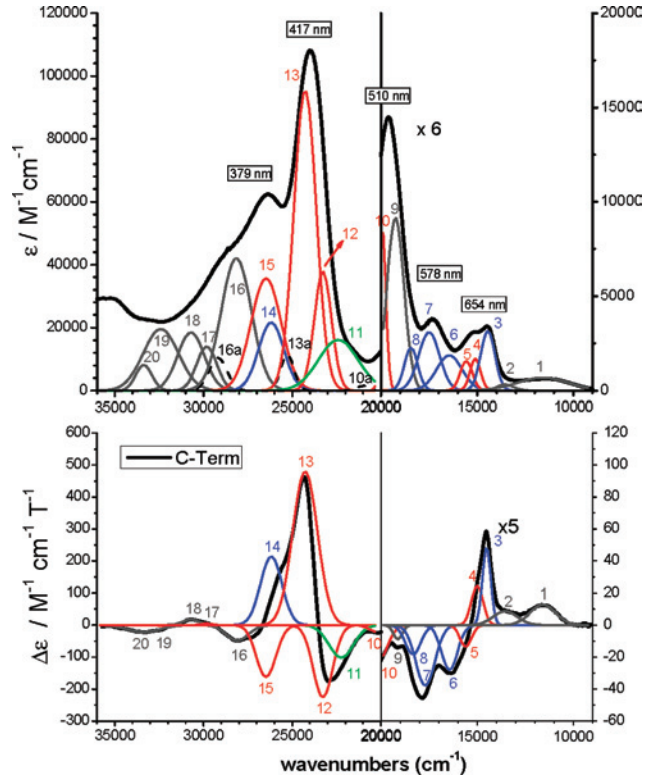

Figure 3. Electronic spectra of [Fe(TPP)(Cl)]. Top: UV−vis absorption spectrum measured in $CHCl_3$ at room temperature. Bottom: MCD **C**-term spectrum measured in PS at 5.8 K (lower concentration for 36 000− 21 000 cm^{-1} region) and 5.6 K (higher concentration for 21 000−9000 cm^{-1}), respectively. The colored lines represent a correlated Gaussian fit of these data (cf. Table 2), where the polarizations are color-coded (in-plane in red, out-of-plane in blue, mixed in green, and not determined in gray).

Scheme 1

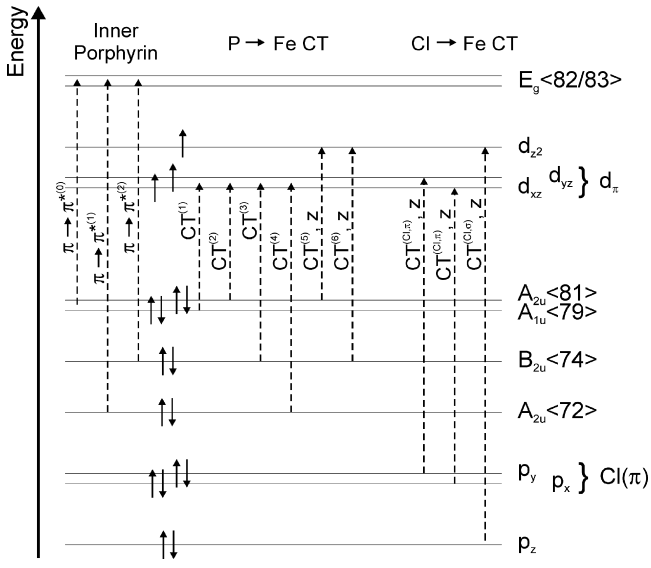

of electronic spectra. In a classic study, Browett et al. determined the axial zfs parameter for [Fe(TPP)(Cl)] (D = 6.9 cm^{-1}) by analyzing MCD saturation curves using low-temperature MCD spectroscopy (at liquid helium temperature).[9] The obtained value for D is in good agreement with D = 6 cm^{-1} as determined from single crystal magnetic susceptibility measurements,[25] and D values from far IR (6.5 cm^{-1})[26a] and Mössbauer (7.0 cm^{-1})[26b] experiments. The fit of the temperature-dependent MCD data also demonstrates that the ground-state is S = 5/2.[9] This is in agreement with EPR results, which show an axial spectrum with g values of $g_\perp \approx 6.06$ and $g_\parallel \approx 2.01$.[9] Hence, E/D is zero. The low-temperature MCD data of [Fe(TPP)(Cl)] presented in Figure 3 are in agreement with the data obtained by Browett et al.[9] The MCD spectrum shows one temperature independent B-term feature at 19084 cm^{-1}, and five sign changes at about 15340, 23530, 26630, 29500, and 31740 cm^{-1}, respectively (cf. Figure 3). The latter two sign changes were not observed by Browett et al.[9] indicating that the data set presented here has a better resolution in the higher energy region. The saturation intensity (peak-to-trough intensity of the Soret band) obtained from the MCD spectrum measured at 1.8 K and +7 T is 3.4 × 10^3 M^{-1} cm^{-1}, which is significantly lower than saturation limits observed for ls ferric heme proteins with S = 1/2 ground states. As shown in Table 3, the saturation intensity observed for the ls compounds is in the range of 25 × 10^3 to 61 × 10^3 M^{-1} cm^{-1}.

Figure 4 presents the high-temperature MCD spectrum of [Fe(TPP)(Cl)] measured at 290 K, which has been determined to quantify temperature-independent **A**- and **B**-term contributions to the total MCD intensity. The two Soret components are observed as a derivative shaped band at 24272 and 23121 cm^{-1}. Because of the nearly degenerate $E_g\langle 82/83\rangle$ (LUMO) orbitals of the TPP^{2-} ligand, the Soret band shows intense **A**-term features with 15 and −11 M^{-1} cm^{-1} T^{-1}, respectively. Q_v is observed as a derivative shaped band at 20202 cm^{-1}, whereas Q is not observed in the spectrum. The molar intensity at 290 K for Q_v is about 0.4 M^{-1} cm^{-1} T^{-1}. Subtraction of the molar 290 K spectrum from the low temperature data yields the corresponding pure **C**-term spectrum shown in Figure 4 and Figure 3, bottom. On the basis of these data, the molar **C**-term intensity of the two major Soret components of [Fe(TPP)(Cl)] is 477 and −182 M^{-1} cm^{-1} T^{-1}, respectively. To perform a reliable analysis of the VTVH **C**-term data, it is of critical importance to subtract the temperature independent **A**- and **B**- term contributions. This especially applies to the Soret band because significant **A**-term contributions are present in this case as shown in Figure 4.

B.2. Assignments. Figures 6−8 show the VTVH saturation curves for the Soret$^{(1)}$ component located at 23266 cm^{-1} (band 12), band 4 at 15000 cm^{-1} ($CT^{(1)}$), and band 6 at 16444 cm^{-1} ($CT^{(Cl,\pi)}$), respectively. For the fitting of these data, the zero field splitting parameter D determined by Browett et al. (D = 6.9 cm^{-1})[9] was used and E/D was set to zero (vide supra). Because the MCD **C**-term spectrum of [Fe(TPP)(Cl)] is very crowded with many overlapping bands, the individual band positions were determined first from a correlated fit of the absorption and **C**-term spectra as shown in Figure 3. In the next step, the VTVH curves were determined for every band at an energy that minimizes overlap with the neighboring bands. Because of this, the

(25) Behere, D. V.; Mitra, S. *Inorg. Chem.* **1979**, *18*, 1723–1724.
(26) (a) Uenoyama, H. *Biochim. Biophys. Acta* **1971**, *230*, 479–481. (b) Dolphin, D. H.; Sams, J. R.; Tsin, T. B.; Wong, K. L. *J. Am. Chem. Soc.* **1978**, *100*, 1711–1718.

Table 2. Correlated Fit of the UV−vis Absorption and MCD Spectra of [Fe(TPP)(Cl)]

	MCD		UV−vis				
no.	position	$\Delta\varepsilon^a$	position	ε^b	calcd.[c]	assignment	polarization from MCD [d]
1	11584	13	11584	680	12329 (5)	$^6A_1 \rightarrow {}^4T_1$	
2	13542	7	13542	312	12910 (6)	$^6A_1 \rightarrow {}^4T_2$	
3	14512	49	14450	3156	11945 (3)	$CT^{(5)}$	*z*
4	15000	24	15100	1696	12329 (5)	$CT^{(1)}$, $\pi \rightarrow \pi^{*(0)}$	*x*,*y*
5	15600	−13	15570	1563	12910 (6)	$CT^{(1)}$, $\pi \rightarrow \pi^{*(0)}$	*x*,*y*
6	16444	−28	16450	1859	20740 (11)	$CT^{(Cl,\pi)}$	*z*
7	17700	−38	17500	3084	22455 (15)	$CT^{(6)}$, $CT^{(Cl,\sigma)}$	*z*
8	18336	−18	18440	2253	22605 (16)	$CT^{(6)}$	*z*
9	(19129)	−9	19250	9163		B-Term signal	
10	20150	−22	19950	8782		Q_v	*x*,*y*
11	22232	−101	22400	16099	25203 (21)	$\pi \rightarrow \pi^{*(1)}$, $CT^{(Cl,\pi)}$	*x*,*y*, and *z*
12	23266	−226	23266	37833	26071 (25)	$\pi \rightarrow \pi^{*(2)}$, $\pi \rightarrow \pi^{*(0)}$ **(Soret)**, $CT^{(4)}$	*x*,*y*
13	24269	479	24270	95604	26143 (27)	$\pi \rightarrow \pi^{*(0)}$ **(Soret)**, $\pi \rightarrow \pi^{*(2)}$	*x*,*y*
14	26181	214	26181	21665	25008 (19)	$CT^{(Cl,\pi,\sigma)}$, $CT^{(5)}$	*z*
15	26472	−162	26472	35635	26109 (26)	$\pi \rightarrow \pi^{*(0)}$ **(Soret)**, $\pi \rightarrow \pi^{*(2)}$, $CT^{(4)}$	*x*,*y*
16	28098	−48	28150	42029	27164 (28)	$\pi \rightarrow \pi^{*(2)}$	
17	29819	5	29819	13963	27250 (29)	$\pi \rightarrow \pi^{*(2)}$	
18	30704	18	30705	18511			
19	32402	−3	32402	19582			
20	33365	−22	33365	8148			

[a] $\Delta\varepsilon$ is given in [M^{-1} cm^{-1} T^{-1}], measured at 5.8 K for bands 11−20 and 5.6 K for bands 1−10. [b] ε is given in [M^{-1} cm^{-1}], measured at room temperature in $CHCl_3$. [c] Calculated with B3LYP/LanL2DZ* (vide supra) using the full TPP ligand without any simplifications (*d*(Fe−Cl) taken from the crystal structure; ref 18). Numbers in parentheses correspond to the numbering of the excited states in Supporting Information Table S2 from TD-DFT. [d] Polarizations were determined from fitting the experimental VTVH data (examples are shown in Figures 6−8).

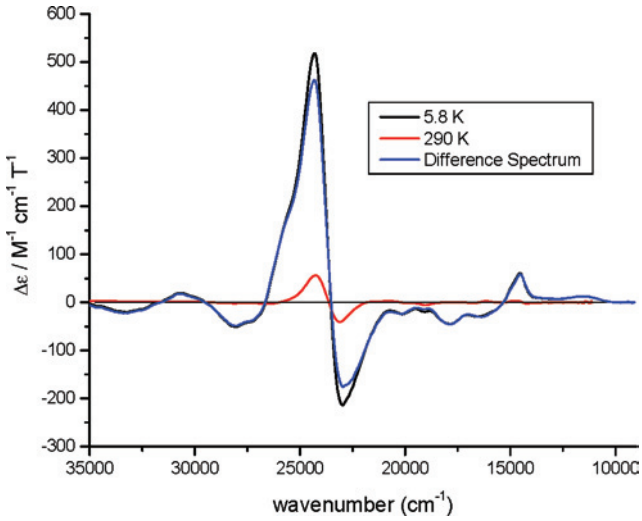

Figure 4. MCD spectrum of [Fe(TPP)(Cl)]: The black line represents the MCD spectrum measured at 5.8 K, and the red line shows the spectrum measured at 290 K. The **C**-term spectrum in blue results from subtraction of the 290 K from the low-temperature data.

Table 3. Peak to Trough Saturation Limits for [Fe(TPP)(Cl)] Compared with Limits Observed in Different Enzymes

compound	spin-state	peak to trough saturation limit[a]	ref
[Fe(TPP)(Cl)	5/2	3.4×10^3	this work
horse heart cytochrome c	1/2	40.5×10^3	ref 35
metmyoglobin CN^-	1/2	60.5×10^3	ref 35
cytochrome c oxidase	1/2	25×10^3	ref 39
cytochrome c oxidase CN^-	1/2	54×10^3	ref 39
ferryl HRP compound I	3/2	1.9×10^3	ref 40

[a] Peak to trough saturation limits are given in M^{-1} cm^{-1}.

specified positions used to obtain the VTVH curves do not necessarily correspond to the particular band maxima. Importantly, *the obtained VTVH curves show two different types of saturation behavior indicating different polarizations*. In-plane (*x*,*y*) polarizations induce a nesting behavior of the corresponding saturation isotherms ("N" behavior:

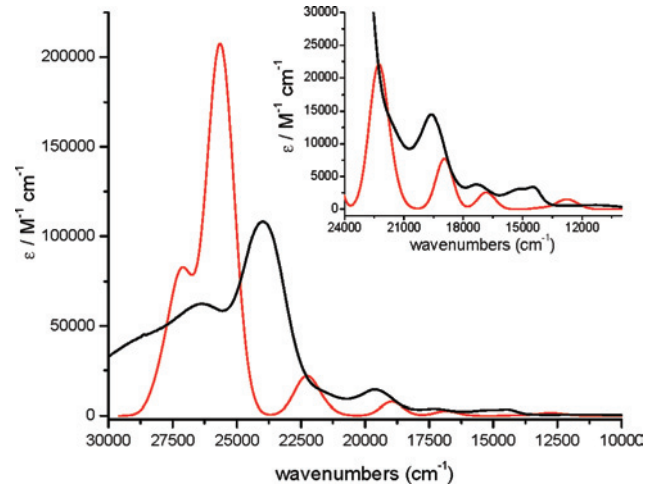

Figure 5. UV−vis absorption spectrum of [Fe(TPP)(Cl)] measured in $CHCl_3$ at room temperature shown in black. The calculated (B3LYP/LanL2DZ*) spectrum is shown in red. The calculated spectrum was obtained using the SWizard program.[41] The bandwidths at half-height were set to 2000 cm^{-1} for the plot.

bands 4, 5, 10, 12, 13, and 15; cf. Figures 6 and 7), whereas out-of-plane (*z*) polarization generates overlaying saturation isotherms ("O" behavior: bands 3, 6, 7, 8, and 14; cf. Figure 8). *This means that the saturation curves allow to clearly distinguish between in-plane and out-of-plane polarized transitions, which is a corner stone for the assignment of all the observed bands* that we identified from the fit shown in Figure 3. For bands 16 and 17, VTVH curves were difficult to obtain because of their low MCD intensities. Hence, their magnetization behavior could not be reliably determined.

On the basis of the experimentally determined polarizations of the electronic transitions and the TD-DFT results, the electronic spectra of [Fe(TPP)(Cl)] can now be assigned for the first time. The UV−vis spectrum in Figure 3 shows the Soret band at about 417 nm and an unusual, broad band

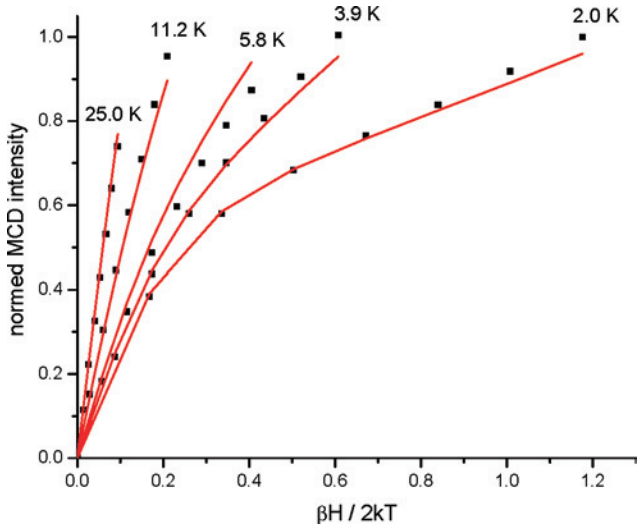

Figure 6. MCD saturation magnetization curves (VTVH) for band 12 (Soret) at 23266 cm^{-1} (red lines: fit; black dots: experimental data points) showing *x*,*y*-polarization.

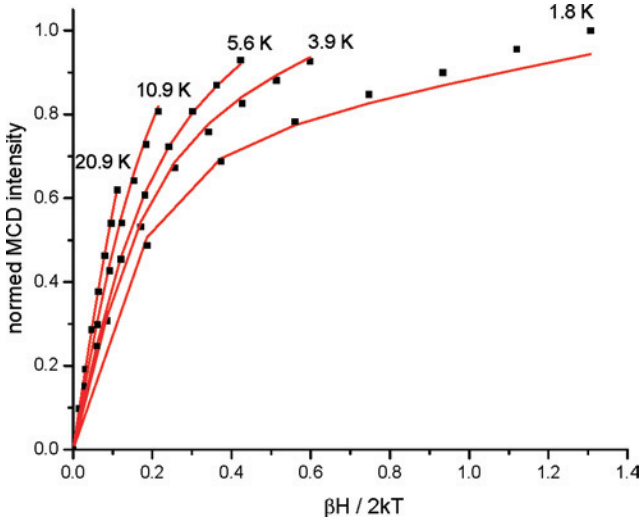

Figure 7. MCD saturation magnetization curves (VTVH) for band 4 ($CT^{(1)}$) at 15000 cm^{-1} (red lines: fit; black dots: experimental data points) showing *x*,*y*-polarization with about 2% *z*-polarization.

to higher energy at 379 nm, which could correspond to a second Soret component. A much better resolution of this spectral region is available from the MCD spectrum, which shows three Soret components at 23266, 24269, and 26472 cm^{-1} (bands 12, 13, and 15), which all exhibit in-plane polarizations. This observation is in agreement with the TD-DFT results, which also show three Soret components (bands 25−27 in Supporting Information Table S2). The appearance of three Soret components instead of the expected two in form of a pseudo-**A** (cf. Discussion) is due to admixture of the $CT^{(4)}$ excited state, which corresponds to the transition from the low-lying $A_{2u}\langle 72 \rangle$ porphyrin orbital ($\beta\langle 156\rangle$; cf. Figures 1 and 2) to the d_π orbitals (d_{xz}, d_{yz}) of iron. In the case of [Fe(TPP)(Cl)], $CT^{(4)}$ is close in energy to the Soret excited state, which induces a CI mixing of these states (both excited states have E_u symmetry in D_{4h}). Hence, the Soret band splits into three components. In the calculation, the band in the middle (band 26 at 27017 cm^{-1}) has mostly $CT^{(4)}$ character. Experimentally, the assignment is different. As

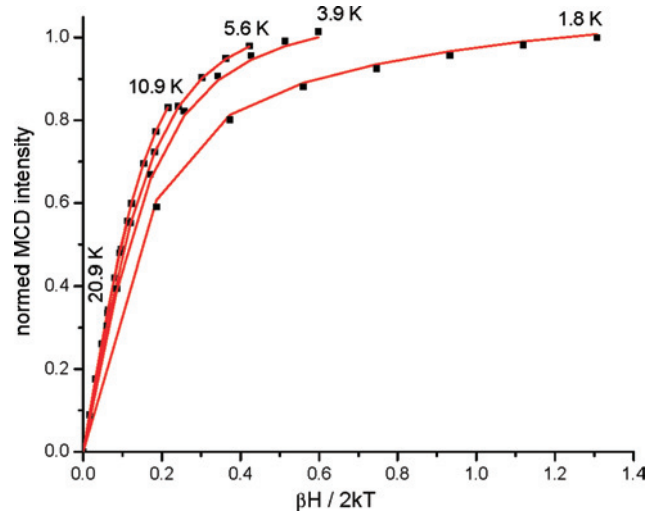

Figure 8. MCD saturation magnetization curves (VTVH) for band 6 ($CT^{(Cl,\pi)}$) at 16444 cm^{-1} (red lines: fit; black dots: experimental data points) showing 77% *z*-polarization with about 23% *x*,*y*-polarization.

further elaborated in the Discussion, the Soret band usually gives rise to a pseudo-**A** in the MCD, where each MCD band corresponds to one component of the low-symmetry split Soret E_u excited state. Importantly, since $CT^{(4)}$ does only have the $A_{2u} \rightarrow E_g$ component, it only mixes with one component of the Soret band, either the positive or the negative **C**-term feature. A quick inspection of Figure 3, bottom, shows that in this case the negative feature is split into two bands (bands 12 and 15), which are therefore assigned to the mixed Soret/$CT^{(4)}$ transitions. Correspondingly, the combined integral intensity of bands 12 and 15 should be roughly equivalent to the other Soret component, band 13. In this respect, please note that the UV−vis and **C**-term intensity ratios of bands 14 and 15 are not well defined from the spectra. In any case, the fact that band 14 does not correspond to another Soret component is evident from its out-of-plane (*z*-) polarization, experimentally determined from the VTVH data of this band. The fit shown in Figure 3 places band 14 at 26181 cm^{-1}. This feature is assigned to the $CT^{(Cl,\pi,\sigma)}$ transition mixed with $CT^{(5)}$. This is in agreement with photoreduction experiments of Hendrickson et al. (see Discussion).[27]

To higher energy of the Soret transition, bands 16 and 17 are assigned to two components of the $\pi \rightarrow \pi^{*(2)}$ transition, which correspond to the excitation of an electron from $B_{2u}\langle 74\rangle$ into the $E_g\langle 82/83\rangle$ orbitals of the porphyrin. The corresponding excited-state has E_u symmetry (in D_{4h}) and hence generates a pseudo **A**-term in the lower symmetry environment of [Fe(TPP)(Cl)] (see Discussion). Correspondingly, bands 16 and 17 have opposite signs in MCD (cf. Figure 3), in agreement with this assignment. To lower energy of the Soret transition, a number of *z*-polarized bands are observed. Band 11 corresponds to the $A_{2u}\langle 81\rangle \rightarrow B_{1u}\langle 84\rangle$ transition, which is Laporte forbidden and hence does not offer oscillator strength. From TD-DFT, the intensity of this band is actually due to 7% $CT^{(Cl,\pi)}$ character (*z*-polarized)

(27) Hendrickson, D. N.; Kinnaird, M. G.; Suslick, K. S. *J. Am. Chem. Soc.* **1987**, *109*, 1243–1244.

and 6% $\pi \rightarrow \pi^{*(1)}$ admixture (*x*,*y*-polarized; cf. Supporting Information Table S2), which combined give rise to the mixed magnetization saturation behavior (O_N) observed experimentally for this feature. Three additional out-of-plane polarized bands are observed at 18336, 17700, and 16444 cm^{-1} (bands 6−8; cf. Table 2), respectively. Band 8 corresponds to the *z*-polarized $B_{2u}\langle 74\rangle \rightarrow d_{z^2}$ transition (90% $CT^{(6)}$; cf. Supporting Information Table S2). Note that this feature is *z*-polarized, because the iron is located above the porphyrin plane toward the axial chloro ligand.[21] Band 6 is assigned to the mixed $CT^{(Cl,\pi)}$ transition, and band 7 to an excitation with mixed $CT^{(6)}$ and $CT^{(Cl,\sigma)}$ character, based on the energy sequence of these transitions in the TD-DFT calculations. Note that for both bands 6 and 7, TD-DFT predicts that the main contribution to the excited states comes from the forbidden $E_g \rightarrow d_\pi$ transition (cf. Supporting Information Table S2). $CT^{(5)}$, which shows z-polarization due to the out-of-plane displacement of the iron, is assigned to band 3 at 14512 cm^{-1} in agreement with the TD-DFT result. The nature of bands 1 and 2 at 11584 and 13542 cm^{-1} in MCD and in UV−vis, respectively, is not entirely clear. Both bands are very weak, so no polarizations could have been determined experimentally. We believe that these two features correspond to the spin-forbidden $^6A_1 \rightarrow {}^4T_1 + {}^4T_2$ ligand field transitions of hs Fe(III), which are usually observed in the 10000−15000 cm^{-1} region. The intensity of these features is certainly quite large for spin-forbidden ligand field transitions. Hence, one possibility is that the corresponding ligand field excited quartet states mix with quartet states that result from porphyrin $\pi \rightarrow \pi^*$ triplet excitations, leading to the observed gain in intensity. Nevertheless, this assignment remains tentative.

Finally, Q_v is observed at 20150 cm^{-1} (band 10) showing in-plane polarization in the MCD spectrum, and at 19950 cm^{-1} in UV−vis. This feature should give rise to a pseudo-**A** in MCD, but no derivative band shape is observed in this case. This is most likely due to the fact that Q_v is really weak in the MCD spectrum of [Fe(TPP)(Cl)], and hence, the other component is likely hidden by excitations with larger **C**-term intensity at low-temperature. On the other hand, Q_v can be identified from the high-temperature data, where a corresponding **A**-term signal is observed at 20202 cm^{-1} (vide supra), indicating that this assignment is correct. This assignment is further supported by rRaman spectroscopy (cf. Discussion). The Q-band is neither observed in MCD nor UV−vis and therefore must be of very low intensity in [Fe(TPP)(Cl)]. Importantly, this is also observed for a number of other metalloporphyrins.[23] For example, four-coordinate ls [Co(TPP)] does not show the Q-band either in MCD or in UV−vis.[28] [Fe(TPP)(NO)] is another example for very weak Q and Q_v bands.[17] Transitions 4 and 5 at 15000 and 15600 cm^{-1}, respectively, are in-plane polarized and therefore assigned to $CT^{(1)}$. Because this excited-state has E_u symmetry in D_{4h}, corresponding to the $A_{1u} \rightarrow d_\pi$ excitation, it shows a pseudo **A**-term in the lower symmetry environment of [Fe(TPP)(Cl)] (see Discussion). Note that from the TD-DFT calculations, this band has also $\pi \rightarrow \pi^{*(0)}$ character (cf. Supporting Information Figure S2). This assignment is further supported by rRaman spectroscopy (see Discussion). The related transition $CT^{(2)}$, corresponding to the $A_{2u} \rightarrow d_\pi$ excitation, is predicted below 9000 cm^{-1}. We were not able to observe this transition within the energy range of our equipment (cut off: 9090 cm^{-1}). The assignments are collected in Table 2.

(28) Paulat, F.; Lehnert, N. manuscript in preparation.

Discussion

In this study, the electronic spectra (MCD and UV−vis) of five-coordinate [Fe(TPP)(Cl)] are analyzed in detail. As evident from Figure 3, and explicitely noticed in the preceding literature,[1c,9,23] the electronic spectra of hs ferric hemes, especially [Fe(TPP)(Cl)], are very complicated and hence could not have been assigned previously. To analyze the electronic spectra, a correlated fit of the absorption and low-temperature MCD data of [Fe(TPP)(Cl)] was performed first, which allows for the identification of at least 20 electronic transitions. Therefore, it is not surprising that an assignment of these data was not possible so far. Since iron has a hs d^5 configuration in [Fe(TPP)(Cl)], d−d transitions are in general spin forbidden. Hence, three different types of electronic transitions are expected for hs ferric porphyrins: porphyrin to metal charge-transfer (P → M CT) transitions, axial ligand to iron CT transitions (here: Cl → M CT), and porphyrin $\pi \rightarrow \pi^*$ transitions (cf. Scheme 1). To obtain further insight into the nature of the different transitions, we measured VTVH **C**-term saturation curves, which allow for the determination of the polarizations of the MCD bands. The VTVH saturation curves obtained this way were then simulated.[2] [Fe(TPP)(Cl)] shows strong axial zfs ($D = 6.9$ cm^{-1})[9] as evident from EPR ($E/D = 0$). Because of this, a large magnetic anisotropy is obtained, and importantly, the magnetization saturation behavior of in-plane and out-of-plane polarized transitions should be dramatically different. In fact, two different types of saturation behavior are found experimentally. The VTVH isotherms for in-plane polarized bands are nested as shown for the Soret band (band 12) in Figure 6. In contrast, for out-of-plane polarized bands, the isotherms are overlaying as shown for $CT^{(Cl,\pi)}$ (band 6) in Figure 8. With the polarizations of all the individual transitions thus known experimentally, TD-DFT calculations have been used to completely assign the spectra. An accurate theoretical description of [Fe(TPP)(Cl)] was obtained from TD-DFT calculations on the B3LYP/LanL2DZ* level. These calculations are not sufficient enough by themselves to assign the spectra, but they supply a number of important pieces to solve the puzzle. The TD-DFT results provide a list of important transitions and their relative energies and intensities with good accuracy, and this way, define the "active space" of electronic transitions that are relevant. Finally, the occurrence of pseudo **A**-terms in the MCD **C**-term spectra is very useful to locate E_u excited states, split in the lower

symmetry of [Fe(TPP)(Cl)] (vide infra).[29] The complete assignments of the UV−vis and MCD spectra of [Fe(TPP)(Cl)] are listed in Table 2. On the basis of these results, we are now able to explain a number of puzzling observations in the absorption spectra of [Fe(TPP)(Cl)], which have gained much interest and caused much confusion in the literature.[2,9,11,23,27,30,31] This includes (a) the nature of the intense, broad band to higher energy of the Soret band, (b) the broad appearance of the Soret band, (c) the position of Q and Q_v, (d) the assignment of the ∼640 nm feature, (e) the position of Cl → Fe CT transitions, and (f) the energies of porphyrin → d_π CT transitions.

As described by Gouterman,[23] the electronic absorption spectra of "normal" metalloporphyrins are quite simple and show the intense Soret, Q, and Q_v bands. Note that Q_v is a vibronic band due to vibronic coupling of the Soret and Q states. As evident from Figure 3, top, a much more complicated situation is encountered for [Fe(TPP)(Cl)]. In the case of the Soret and Q transitions, we have derived theoretically that these features should give rise to a pseudo-**A** signal in the low-temperature MCD **C**-term spectrum.[17,29] This is due to the fact that the corresponding excited Soret and Q states have E_u symmetry, but the degeneracy is slightly lifted because of the lower symmetry of the metalloporphyrins.[32] Both resulting components of these E_u states then spin−orbit couple, leading to the appearance of the pseudo-**A** signal.[29] As shown in Figure 3, bottom, the MCD **C**-term spectrum of [Fe(TPP)(Cl)] does *not* show the predicted pseudo-**A** term for the Soret band. In contrast, four different features (bands 12−15) are observed in the Soret region by MCD. What are the assignments of these features? First, analysis of the VTVH saturation behavior of these bands shows that band 14 is *z*-polarized, and hence, cannot correspond to a Soret component (vide infra). From the saturation behavior and the TD-DFT results, the remaining bands 12, 13, and 15 are in fact Soret components. But why are there three instead of the expected two features? This is due to the fact that in [Fe(TPP)(Cl)], the Soret band is mixed with the porphyrin $A_{2u}\langle 72\rangle \rightarrow E_g\langle 82/83\rangle$ ($\pi \rightarrow \pi^{*(1)}$) transition, which also gives rise to an E_u excited state. However, there is one important difference to the Soret state: whereas the Soret excited-state has both $A_{1u}\langle 79\rangle \rightarrow E_g\langle 82/83\rangle$ and $A_{2u}\langle 81\rangle \rightarrow E_g\langle 82/83\rangle$ contributions, $\pi \rightarrow \pi^{*(1)}$ only has the $A_{2u}\langle 72\rangle \rightarrow E_g\langle 82/83\rangle$ component. Hence, $\pi \rightarrow \pi^{*(1)}$ mixes selectively with *one component* of the Soret band, in this case the negative MCD feature, which is split into two negative components giving rise to bands 12 and 15. The positive Soret component is unaffected, giving rise to band 13. This is in agreement with the TD-DFT results. Additional information that confirms these assignments is available from rRaman spectroscopy. In a recent publication by our group, the rRaman spectra of [Fe(TPP)(Cl)] have been investigated.[21] The rRaman spectrum of [Fe(TPP)(Cl)] excited at 454.5 nm shows mostly totally symmetric (A_{1g}) vibrations corresponding to Raman ***A***-term enhancement,[33] and therefore, the absorption band at 417 nm has been assigned to the Soret band. This is in agreement with the assignments presented here.

Researchers have been speculating for a long time about the nature of the broad band at 379 nm (cf. Figure 3). Our results show that one component of this feature (band 15) corresponds to the split Soret band as described above. Importantly, the MCD VTVH isotherms for the other component, band 14 at 26181 cm^{-1}, show *z*-polarization. This band is therefore assigned to the chloride to Fe $CT^{(Cl,\pi,\sigma)}$ transition mixed with $CT^{(5)}$ (cf. Table 2) in agreement with TD-DFT. This is also in agreement with work by Hendrickson et al.,[27] who observed that irradiation into the near-ultraviolet band at ∼379 nm in [Fe(TPP)(X)] (X = F^-, Cl^-, Br^-, I^-, and N_3^-) leads to rapid photoreduction of the iron atom and generation of a (pseudo) halide radical, and therefore assigned this band as a (pseudo) halide ligand to Fe CT. This assignment leads to another interesting question: do the Cl to Fe CT transitions give rise to other distinct features besides band 14? This question is easy to address by MCD because these transitions are *z*-polarized. Analysis of the data shows that there are additional bands (bands 6, 7, and 11; cf. Table 2) observed with $CT^{(Cl,\pi,\sigma)}$ character, evident from MCD and TD-DFT. Correspondingly, the absorption feature at 578 nm has to be considered as a chloro to Fe CT band.

As mentioned above, the Q and Q_v excited states also have E_u symmetry in D_{4h}, and correspondingly, these should also generate pseudo **A**-terms in the low-temperature MCD spectra. However, no such features are observed. Since Q and Q_v usually give rise to weak features in the MCD **C**-term spectra, this result is not surprising, considering the additional intense bands observed for [Fe(TPP)(Cl)] in this energy region. However, Q_v is readily identified in the high-temperature MCD spectrum of [Fe(TPP)(Cl)], where Q_v gives rise to an **A**-term at 20202 cm^{-1}. A closer inspection of the **C**-term MCD spectrum then reveals one component of Q_v at 20150 cm^{-1} (band 10, cf. Table 2), showing the expected in-plane polarization. Because of the very low intensity of Q in [Fe(TPP)(Cl)], this band is neither observed in MCD nor UV−vis. On the other hand, rRaman spectroscopy is a powerful tool to identify Q and Q_v in metalloporphyrins. Both Q and Q_v lead to Raman ***B***-term enhancement related to vibronic coupling, which is manifested in the enhancement of anomalous polarized A_{2g} modes, as well as B_{1g} and B_{2g} vibrations.[30,31] The rRaman spectrum of [Fe(TPP)(Cl)] excited at 568.2 nm shows weak, and the data obtained at 514.5 nm show medium intense anomalous polarized bands indicating vibronic coupling.[21] In addition, overtones are enhanced upon excitation into the absorption band at 510 nm, which indicates that this band actually corresponds to

(29) Lehnert, N. In *The Smallest Biomolecules: Diatomics and their interactions with heme proteins*; Ghosh, A., Ed.; Elsevier: Amsterdam, 2008; pp 147–172.

(30) Spiro, T. G.; Li, X.-Y. In *Resonance Raman Spectra of Heme and Metalloproteins*; Spiro, T. G., Ed.; Wiley: New York, 1988; pp 1−37.

(31) Spiro, T. G. In *Iron Porphyrins*; Lever, A. B. P., Gray, H. B., Eds.; Addison-Wesley: Reading, MA, 1983; Part *2*, pp 89−159.

(32) The splitting of the Soret E_u state can only be determined from MCD, and is usually in the range of 300−1500 cm^{-1}.

(33) Czernuszewicz, R. S.; Spiro, T. G. In *Inorganic Electronic Structure and Spectroscopy*; Solomon, E. I., Lever, A.B. P., Eds.; John Wiley & Sons: New York, 1999; Vol. *1*, pp 353−441.

Q_v. This latter assignment is in very good agreement with the high-temperature MCD data, which reveal Q_v at 20202 cm^{-1}. On the basis of the rRaman results, Q should be located in the 18000−19000 cm^{-1} range. However, this would lead to an energy separation of Q and Q_v of about 2350 cm^{-1}, which is too large. It should only be about 1250 cm^{-1} as determined by Gouterman.[23] Hence, the Q-band is very weak in [Fe(TPP)(Cl)] both in absorption and MCD and not observed spectroscopically. This feature is likely masked by the intense band at 578 nm (band 7; cf. Figure 3), which, however, is *z*-polarized, and therefore, cannot correspond to Q (vide supra).

Another interesting feature in the electronic spectra of [Fe(TPP)(Cl)] is the low-energy band at 654 nm, which is quite intense in absorption. The nature of this band has led to much discussion in the literature in the past.[11,23,30,31] In earlier work, we found that rRaman excitation at 647.1 nm not only shows the usually observed porphyrin A_{2g} modes at 1335 and 1522 cm^{-1} indicative of vibronic coupling, but also low-energy anomalous polarized bands that are not observed at any other excitation wavelength. These low-energy bands correspond to in-plane and out-of-plane porphyrin deformation modes with some phenyl out-of-plane mode contribution. Hence, the absorption band at 654 nm shows a completely different excitation behavior as usually observed for Q and Q_v band enhancements. On the basis of this, we concluded that this absorption band should correspond to a P → Fe CT transition.[21] This result is now confirmed by MCD spectroscopy, which allows to assign the corresponding bands 4 and 5 (cf. Figure 3) to the $A_{1u}\langle 79\rangle \rightarrow d_\pi$ transition ($CT^{(1)}$). Because this excitation leads to an excited-state with E_u symmetry, a pseudo-**A** signal is observed for bands 4 and 5 in agreement with this assignment. We believe that the enhancement of out-of-plane deformation modes of A_{2g} symmetry relates to the fact that $CT^{(1)}$ corresponds to a one electron transition from the $A_{1u}\langle 79\rangle$ HOMO of the porphyrin into the d_π orbitals of iron. This generates a porphyrin π-cation radical electronic structure in the excited state. Crystallographic data for the π-cation radical complex [Zn(TPP)(ClO_4)] show a strongly ruffled porphyrin core with large out of plane distortions.[34] Hence, the observed enhancement of porphyrin deformation modes is indicative of large structural changes of the porphyrin core following the $CT^{(1)}$ excitation (vibronic coupling to the geometry-relaxed state?). Taken together, these results therefore allow us to unambiguously assign the 654 nm absorption band of [Fe(TPP)(Cl)] to porphyrin to iron CT transitions. One component, bands 4 and 5, correspond to the $A_{1u} \rightarrow d_\pi$ transition, the exact location of which has therefore finally been determined. A second component, band 3, is *z*-polarized and of $A_{2u} \rightarrow d_{z^2}$ type.

On the basis of the detailed analysis of the MCD data of [Fe(TPP)(Cl)] presented here, we were therefore able to address all open questions about the electronic spectra of this complex. As mentioned in the Introduction, the only other effort to assign parts of the MCD spectra of [Fe(TPP)(Cl)] came from Kobayashi and co-workers.[11] In this study, the lowest excited sextet state energies of [Fe(TPP)(Cl)] were calculated from empirical molecular parameters, which were mostly derived from spectral data of related metalloporphyrins. The electronic spectra of [Fe(TPP)(Cl)] were then explained based on the configuration interaction of the porphyrin excited triplet and singlet states ($\pi \rightarrow \pi^{*(0)}$) and $CT^{(1,2)}$. However, the strong contribution of triplet states in the chosen model, which means that they are a main contributor to the electronic spectra of [Fe(TPP)(Cl)], is very doubtful. No corresponding transitions are observed for [Co(TPP)] and other simple metalloporphyrins. Second, the transitions generated this way are all *xy*-polarized, whereas the experimental data show many *z*-polarized bands in the low energy region, which this model cannot account for. Finally, the number of transitions involved is much too small, in particular, no chloro to Fe CT has been considered. The assignments presented here are in agreement with all available experimental data.

Scheme 2

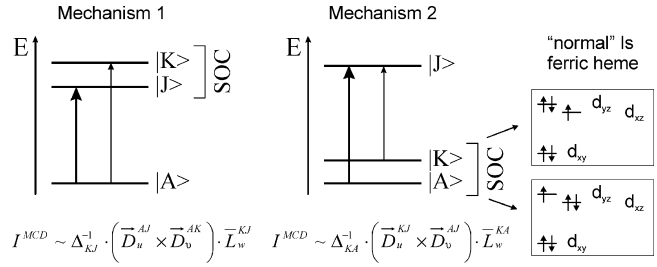

Interestingly, the observed MCD saturation intensity for hs [Fe(TPP)(Cl)] is one order of magnitude smaller compared to ls ferric heme. Table 3 summarizes the peak to trough saturation limits for a number of ferric hemes in different spin states. For example, horse heart cytochrome c shows a value of 40.5×10^3 M^{-1} cm^{-1},[35] whereas [Fe(TPP)(Cl)] exhibits only 3.4×10^3 M^{-1} cm^{-1}. This dramatic difference is due to different spin orbit coupling (SOC) mechanisms in the hs and ls complexes. Scheme 2 shows the two different mechanisms for **C**-term intensity,[2] either based on SOC between two excited states (mechanism 1), or the ground-state and a low lying excited state (mechanism 2). Whereas mechanism 1 is valid for all iron(III) porphyrins, the ls state also has contributions from mechanism 2 because of the low lying excited states generated from the $[t_{2(g)}]^5$ electron configuration that do not exist in the hs state. For ls ferric hemes with the "normal" ground-state as indicated in Scheme 2, very strong SOC exists between the ground-state and the first excited-state corresponding to the reduced SOC matrix element $\langle d_{xz}|l_z|d_{yz}\rangle$. This leads to a dramatic increase in MCD intensity compared to the hs state. The fact that mechanism 2 is in fact responsible for this increase in MCD intensity of *xy*-polarized transitions is evident from MCD data of ls ferric hemes with the alternative "d_{xy}" ground state ($[d_{xz},d_{yz}]^4$ $[d_{xy}]^1$).[36] In this case, no SOC effective in the *z* direction is

(34) (a) Spaulding, L. D.; Eller, P. G.; Bertrand, J. A.; Felton, R. H. *J. Am. Chem. Soc.* **1974**, *96*, 982–987. (b) Song, H.; Rath, N. P.; Reed, C. A.; Scheidt, W. R. *Inorg. Chem.* **1989**, *28*, 1839–1847. (c) Vangberg, T.; Lie, R.; Ghosh, A. *J. Am. Chem. Soc.* **2002**, *124*, 8122–8130.

(35) Thomson, A. J.; Johnson, M. K. *Biochem. J.* **1980**, *191*, 411–420.

present, and hence, mechanism 2 cannot contribute. Correspondingly, the MCD spectra obtained by Cheesman et al. for a complex with "d_{xy}" ground-state show a dramatic decrease in MCD intensity compared to "normal" ls ferric hemes.[37] This difference in SOC is also indirectly reflected by the fact that ls-Fe(III) shows large *g* shifts, whereas hs Fe(III) has practically no *g* shifts at all.[38]

Conclusions

In summary, reliable assignments of the electronic spectra of [Fe(TPP)(Cl)] have been obtained in this work based on detailed analyses of MCD data correlated to TD-DFT calculations. These assignments are confirmed by other methods, especially rRaman. On the basis of these results, an accurate theoretical description of the ground and excited states of [Fe(TPP)(Cl)] has been obtained for the first time. This study demonstrates the impact of low-temperature MCD spectroscopy for the analysis and assignment of electronic spectra of paramagnetic transition metal complexes. In future studies, we will apply this methodology to hs ferric hemes in proteins, especially cytochrome P450.

Acknowledgment. Financial support of this work was provided by the Deutsche Forschungsgemeinschaft (DFG; Grant LE 1393/1-2) which is gratefully acknowledged. F.P. acknowledges the Fonds der Chemischen Industrie (FCI) for a Chemiefonds fellowship.

Supporting Information Available: Method calibration (TD-DFT), complete ref 16, tables of the calculated (TD-DFT, INDO/S−CI) energies for the Soret and Q bands of [Zn(P)] and [Zn(TPP)], assignments of the calculated spectra (TD-DFT) of [Fe(TPP)(Cl)], and coordinates and figures of the fully optimized structure of [Fe(TPP)(Cl)] (PDF). This material is available free of charge via the Internet at http://pubs.acs.org.

IC8002838

(36) Walker, F. A. *Chem. Rev.* **2004**, *104*, 589–615.
(37) Cheesman, M. R.; Walker, F. A. *J. Am. Chem. Soc.* **1996**, *118*, 7373–7380.
(38) Walker, F. A. *Coord. Chem. Rev.* **1999**, *185−186*, 471–534.
(39) Thomson, A. J.; Johnson, M. K.; Greenwood, C.; Gooding, P. E. *Biochem. J.* **1981**, *193*, 687–697.
(40) Browett, W. R.; Gasyna, Z.; Stillman, M. J. *J. Am. Chem. Soc.* **1988**, *110*, 3633–3640.
(41) Gorelsky, S. I. *SWizard program*; University Of Ottawa: Canada, 2007; http://www.sg-chem.net/.